



Cite this: *Phys. Chem. Chem. Phys.*,
2024, 26, 16048

Benchmark *ab initio* characterization of the complex potential energy surfaces of the $\text{HOO}^- + \text{CH}_3\text{Y}$ [Y = F, Cl, Br, I] reactions†

Domonkos A. Tasi * and Gábor Czakó *

The α -effect is a well-known phenomenon in organic chemistry, and is related to the enhanced reactivity of nucleophiles involving one or more lone-pair electrons adjacent to the nucleophilic center. The gas-phase bimolecular nucleophilic substitution ($\text{S}_{\text{N}}2$) reactions of α -nucleophile HOO^- with methyl halides have been thoroughly investigated experimentally and theoretically; however, these investigations have mainly focused on identifying and characterizing the α -effect of HOO^- . Here, we perform the first comprehensive high-level *ab initio* mapping for the $\text{HOO}^- + \text{CH}_3\text{Y}$ [Y = F, Cl, Br and I] reactions utilizing the modern explicitly-correlated CCSD(T)-F12b method with the aug-cc-pVnZ [$n = 2-4$] basis sets. The present *ab initio* characterization considers five distinct product channels of $\text{S}_{\text{N}}2$: ($\text{CH}_3\text{OOH} + \text{Y}^-$), proton abstraction ($\text{CH}_2\text{Y}^- + \text{H}_2\text{O}_2$), peroxide ion substitution ($\text{CH}_3\text{OO}^- + \text{HY}$), $\text{S}_{\text{N}}2$ -induced elimination ($\text{CH}_2\text{O} + \text{HY} + \text{HO}^-$) and $\text{S}_{\text{N}}2$ -induced rearrangement ($\text{CH}_2(\text{OH})\text{O}^- + \text{HY}$). Moreover, besides the traditional back-side attack Walden inversion, the pathways of front-side attack, double inversion and halogen-bond complex formation have also been explored for $\text{S}_{\text{N}}2$. With regard to the Walden inversion of $\text{HOO}^- + \text{CH}_3\text{Cl}$, the previously unaddressed discrepancies concerning the geometry of the corresponding transition state are clarified. For the $\text{HOO}^- + \text{CH}_3\text{F}$ reaction, the recently identified $\text{S}_{\text{N}}2$ -induced elimination is found to be more exothermic than the $\text{S}_{\text{N}}2$ channel, submerged by $\sim 36 \text{ kcal mol}^{-1}$. The accuracy of our high-level *ab initio* calculations performed in the present study is validated by the fact that our new benchmark 0 K reaction enthalpies show excellent agreement with the experimental data in nearly all cases.

Received 11th March 2024,
Accepted 6th May 2024

DOI: 10.1039/d4cp01071j

rscl.li/pccp

1. Introduction

Theoretical and experimental investigations of the gas-phase bimolecular nucleophilic substitution ($\text{S}_{\text{N}}2$) reactions have gained increasing prominence since the 1970s.^{1–10} In step with the progress of computational chemistry and experimental methodology,^{11–16} the initially conceived simple picture of the elemental $\text{S}_{\text{N}}2$ reactions has been found to be incomplete, as it became apparent that along with the traditional Walden inversion and front-side attack, several alternative mechanisms may also occur depending on the reactants and the reaction conditions.^{17–21}

Transcending the conventional reactions between halide ions and methyl halides, our understanding of $\text{S}_{\text{N}}2$ was also

reshaped by the examination of reactions involving HO^- .^{22–38} In 2002, Sun *et al.* investigated the $\text{HO}^- + \text{CH}_3\text{F}$ $\text{S}_{\text{N}}2$ reaction by performing direct dynamics simulations and revealed that the reaction avoids the region of the deep H-bonded $\text{CH}_3\text{OH} \cdots \text{F}^-$ minimum in the exit channel.²² Since then, other theoretical studies have uncovered a novel oxide ion substitution for the $\text{HO}^- + \text{CH}_3\text{F}$ reaction utilizing quasi-classical trajectory (QCT), as well as, direct dynamics calculations.^{39–41} Over the years, the primary focus has been on the dynamical characterization of the $\text{HO}^- + \text{CH}_3\text{I}$ reaction.^{42–48} Wester and co-workers examined several $\text{S}_{\text{N}}2$ reactions experimentally, including $\text{HO}^- + \text{CH}_3\text{I}$, with the crossed-beam ion-imaging technique.^{10,14,49} Direct dynamics simulations were also performed by Hase and co-workers, paving the way for comprehensive experimental-theoretical studies of the $\text{HO}^- + \text{CH}_3\text{I}$ reaction.^{50–52} Furthermore, the present authors developed several global analytical *ab initio* potential energy surfaces (PESs) for $\text{HO}^- + \text{CH}_3\text{I}$ at seven different levels of theory using the in-house ROBOSURFER program package.^{53,54} Afterwards, on the final PES, which was confirmed to be the most suitable for further investigations, more than half a million trajectories were computed, comparing the results with the results of revised crossed-beam experiments

MTA-SZTE Lendület Computational Reaction Dynamics Research Group,
Interdisciplinary Excellence Centre and Department of Physical Chemistry and
Materials Science, Institute of Chemistry, University of Szeged, Rerrich Béla tér 1,
Szeged H-6720, Hungary. E-mail: dtasi@chem.u-szeged.hu,
gczako@chem.u-szeged.hu

† Electronic supplementary information (ESI) available: Benchmark Cartesian coordinates (\AA) and energies (E_{h}) of the stationary points. See DOI: <https://doi.org/10.1039/d4cp01071j>



in order to analyze the dynamics of the reaction in a more detailed manner.⁵⁵ Recently, the mode specificity in the dynamics of the reaction was also studied at several collision energies by exciting certain vibrational modes of the reactants.^{56,57}

Besides considering di- or polyatomic 'normal' nucleophiles (e.g., HO[−], CN[−], NH₂[−], PH₂[−] etc.),^{10,24,58–63} a significant emphasis has been placed on α -nucleophiles (e.g., HOO[−], ClO[−], BrO[−], CH₃OO[−], HOHN[−], NH₂O[−], etc.) participating in S_N2 reactions.^{8,9,64–71} In the case of these α -nucleophiles, one or more lone-pair electrons are located on the atom adjacent to the nucleophilic center, inducing enhanced reactivity compared to that expected from the Brønsted-type correlation.⁷² This phenomenon is known as the α -effect.⁷³ While the existence of the α -effect was beyond doubt in solution, the situation was not as clearly defined in the gas phase.^{72,74,75} By comparing the branching ratios for the reactions of HO[−] and HOO[−] with methyl formate, DePuy and co-workers concluded that HOO[−] does not show the α -effect in the gas phase.⁷⁶ In addition, Villiano *et al.* unveiled that a noticeable α -effect cannot be observed for the HOO[−]/ClO[−]/BrO[−] + CH₃R (R = CH₃, CH₃CH₂, etc.) systems, as well.⁶⁵ In contrast, the opposite of these findings has been confirmed, and several studies have verified that the α -effect stems from the intrinsic properties of α -nucleophiles validating the manifestation of this phenomenon in the gas phase.^{77–85} However, the identification of these intrinsic properties of α -nucleophiles remained disputed.^{86–93} Recently, Hamlin *et al.* reported an extensive theoretical survey on the origin of the α -effect in the gas phase.⁷¹ They employed the activation strain model of reactivity in combination with Kohn–Sham molecular orbital theory and arrived at the conclusion that the adjacent atom of α -nucleophiles induces a reduction in Pauli repulsion between the reactants by polarizing orbital density away from the nucleophilic center. As a result, an enhancement of the reactivity can be obtained for α -nucleophiles compared to their 'normal' counterparts.

Regarding S_N2 reactions involving HOO[−], several theoretical investigations have concentrated on the stationary-point and dynamical characterization, as well.^{74,88,94–97} In the course of the aforementioned α -effect examinations, the stationary points of the corresponding Walden-inversion pathways were determined for several S_N2 reactions of HOO[−] at various levels of theory. The HOO[−]⋯CH₃Y → [HOO⋯CH₃⋯Y][−] → CH₃OOH⋯Y[−] path was explored by Evanseck *et al.* for Y = Cl at the level of HF/6-31+G(d).⁷⁴ Later, in the theoretical surveys of Ren *et al.*, the geometries of the [HOO⋯CH₃⋯Y][−] transition states were optimized in the case of Y = F and Cl at the MP2/6-31+G(d) level of theory, and the corresponding energies were determined with the G2(+) method.^{78,79} Associated with the microsolvated variants of the HOO[−] + CH₃Cl S_N2 reaction, the unsolvated Walden-inversion pathways were also characterized in the studies of Thomsen *et al.*⁸⁸ and Hu *et al.*⁹⁷ utilizing the MP2/6-311++G(d,p) level of theory in combination with G3 and CCSD(T)/aug-cc-pVTZ energy calculations, respectively. The most thorough *ab initio* mapping was achieved by Wu *et al.* in the case of the HOO[−](H₂O)_n + CH₃Y [Y = F, Cl, Br, I; n = 0, 1, 2]

S_N2 reactions, whereby they identified two H-bonded stationary points in the entrance channel, as well.⁹⁶ The dynamics of the HOO[−](H₂O)_n + CH₃Cl reactions, where n = 0 or 1, was also examined with direct dynamics simulations.^{94,95} It is noteworthy that, based on the earlier work of Anick *et al.*,⁹⁸ the only stable structure for the singly hydrated hydroperoxide ion is HO[−](HOH), which indicates that in the S_N2 reaction with CH₃Cl, two distinct pathways may be possible, leading to the CH₃OOH + Cl[−] + H₂O and CH₃OH + Cl[−] + H₂O₂ products. Recently, dynamics simulations performed by Zhao *et al.*⁹⁵ have substantiated that both reaction routes are viable, indicating the fact that a single solvent water molecule can induce a new nucleophile in S_N2 reactions, which opens the door for an alternative pathway. Moreover, for the unsolvated HOO[−] + CH₃Cl reaction, similar to the case of ClO[−] + CH₃Cl,^{65,69} a novel non-S_N2 pathway generating the CH₂O + HCl + HO[−] products was also unveiled. Besides the dynamical description, the PES of the considered product channels of the HOO[−] + CH₃Cl reaction was mapped at the MP2/6-31+G(d,p) level of theory.⁹⁵

In the present work, based on the prominent attention paid to the S_N2 reactions involving hydroperoxide ions, we perform a comprehensive benchmark *ab initio* characterization of HOO[−] + CH₃Y [Y = F, Cl, Br and I] using the explicitly-correlated CCSD(T)-F12b method with the aug-cc-pVnZ [n = 2 (D), 3 (T) and 4 (Q)] basis sets. Besides the traditional Walden-inversion path, we analyze the halogen-bonded complex mechanism⁴⁸ and the possible S_N2 retention routes of front-side attack and double inversion.¹⁹ We identify the stationary points of the proton-abstraction channel, as well; furthermore, relying on the previous study of Xie and co-workers,⁹⁵ our high-level stationary-point mapping also considers other possible pathways. Detailed insights into the applied *ab initio* methods can be found in Section II. In the subsequent Section III, a comprehensive description and discussion of the results are presented, followed by a brief summary of the work in Section IV.

II. Computational details

The stationary points of the title reactions are searched and preoptimized using the second-order Møller–Plesset perturbation theory (MP2)⁹⁹ with the augmented correlation-consistent polarized-valence-double- ζ (aug-cc-pVDZ) basis set.¹⁰⁰ The exploration of the stationary points was conducted based on previous studies and chemical intuition;^{24,38,95} nevertheless, it is important to note that automated methods and approaches for identifying reaction pathways and stationary points in chemical reactions are becoming more and more prevalent.^{101–103} Thereafter, in order to attain more accurate geometries, energies and harmonic frequencies for the stationary points, the explicitly-correlated coupled-cluster singles, doubles, and perturbative triples (CCSD(T)-F12b) method^{104–106} is utilized with the aug-cc-pVDZ and aug-cc-pVTZ basis sets.¹⁰⁰ To achieve a more in-depth mapping, intrinsic reaction coordinate (IRC) computations are also carried out from the saddle points at the MP2/aug-cc-pVDZ level of theory. In order to avoid any spurious stationary point, it is



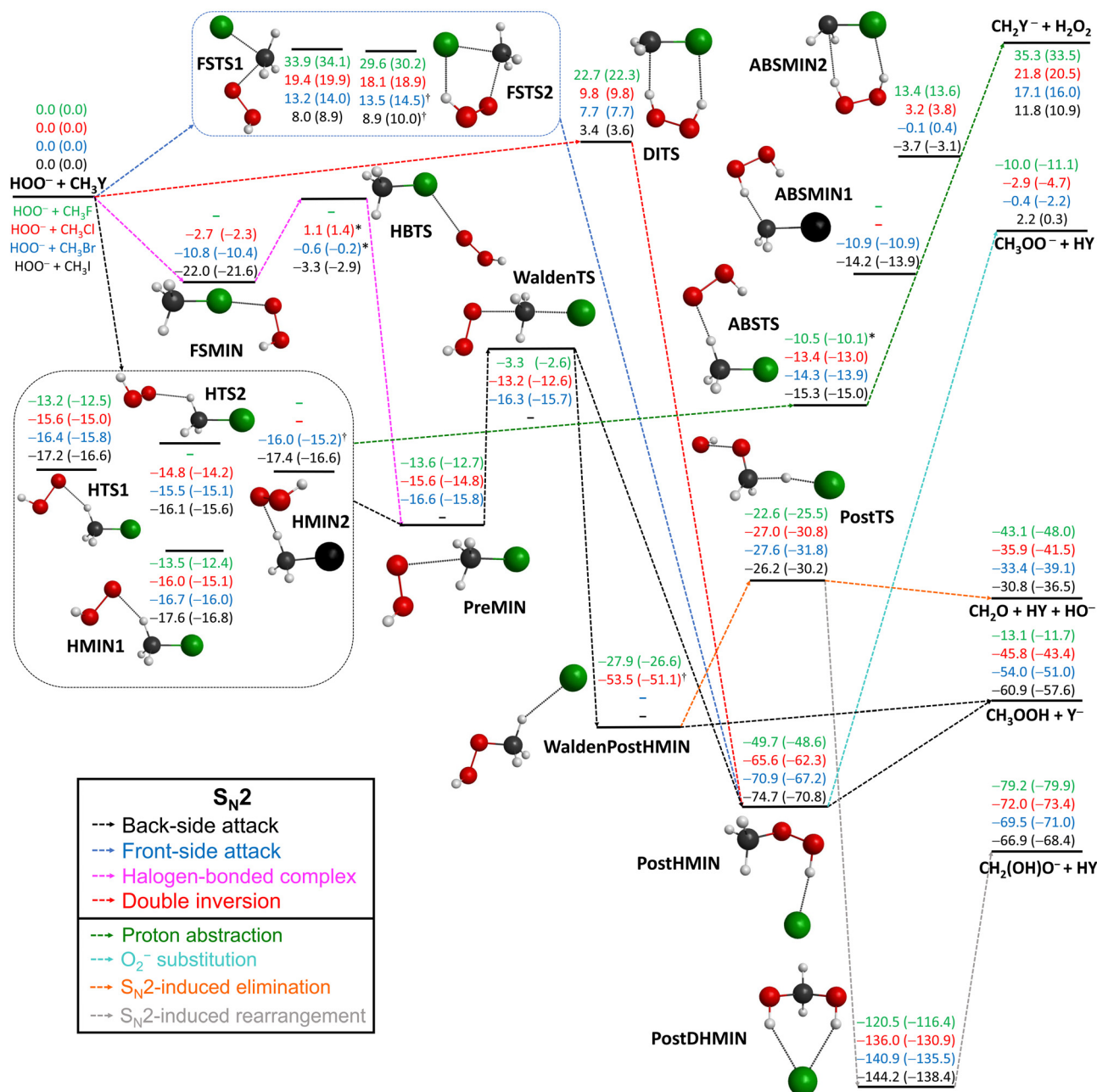


Fig. 1 Schematic representation of the complex potential energy surfaces of the $\text{HOO}^- + \text{CH}_3\text{Y}$ [$\text{Y} = \text{F}, \text{Cl}, \text{Br}, \text{I}$] reactions presenting the classical (adiabatic) CCSD(T)-F12b/aug-cc-pVQZ (+ $\Delta\text{ZPE}[\text{CCSD(T)-F12b/aug-cc-pVTZ}]$) relative energies (kcal mol⁻¹) of the stationary points along the possible reaction routes. [†]MP2/aug-cc-pVDZ structure; *CCSD(T)-F12b/aug-cc-pVDZ structure.

important to note that for all geometry optimizations, the default (3×10^{-4}) required accuracy of the optimized gradient is changed to 10^{-5} in atomic units. Small-core relativistic effective core potentials (ECPs)¹⁰⁷ are employed for Br and I, and the aug-cc-pVnZ-PP [$n = 2-4$] basis sets are applied to replace the inner-core $1s^2 2s^2 2p^6$ (Br) and $1s^2 2s^2 2p^6 3s^2 3p^6 3d^{10}$ (I) electrons. For the stationary points identified in the present work, the computed T_1 -diagnostic values are below 0.02 in every case, except for FSTS and FSTS2 (see Fig. 1), where the values are between 0.02 and 0.04, validating that the multi-reference character is

not a probable issue for the $\text{HOO}^- + \text{CH}_3\text{Y}$ [$\text{Y} = \text{F}, \text{Cl}, \text{Br}$ and I] systems. The benchmark classical (adiabatic) relative energies are computed for the CCSD(T)-F12b/aug-cc-pVTZ structures as follows:

$$\Delta E[\text{CCSD(T)-F12b/aug-cc-pVQZ}] (+\Delta\text{ZPE}[\text{CCSD(T)-F12b/aug-cc-pVTZ}]), \quad (1)$$

where ΔZPE is the harmonic zero-point energy correction. The *ab initio* calculations are performed with the MOLPRO program package.¹⁰⁸



Table 1 Benchmark classical and adiabatic energies (kcal mol^{−1}) of the stationary points relative to the reactants for the possible pathways of the HOO[−] + CH₃Y [Y = F, Cl, Br, I] reactions

HOO [−] + CH ₃ F	MP2	CCSD(T)-F12b			ΔZPE^e	Adiabatic ^f
	DZ ^a	DZ ^b	TZ ^c	QZ ^d		
HMIN1	−14.41	−13.95	−13.69	−13.47	1.09	−12.38
HTS1	−14.00	−13.49	−13.32	−13.15	0.67	−12.49
PreMIN	−14.45	−14.01	−13.80	−13.59	0.84	−12.74
WaldenTS	−6.77	−3.37	−3.44	−3.27	0.66	−2.61
FSTS1	29.87	33.40	33.50	33.87	0.25	34.12
FSTS2	25.76	29.26	29.28	29.64	0.59	30.23
DITS	21.68	21.81	22.37	22.72	−0.37	22.35
PostHMIN	−53.64	−50.43	−49.99	−49.74	1.11	−48.63
WaldenPostHMIN	−32.77	−28.62	−28.08	−27.91	1.26	−26.65
ABSTS	−11.38	−11.00	−10.71 ^g	−10.52 ^g	0.44 ^g	−10.08 ^g
ABSMIN2	12.34	12.43	13.00	13.37	0.28	13.65
PostTS	−28.42	−23.65	−22.93	−22.62	−2.89	−25.51
PostDHMIN	−127.02	−121.31	−120.63	−120.45	4.07	−116.38
HOO [−] + CH ₃ Cl	MP2 ^a	DZ ^b	TZ ^c	QZ ^d	ΔZPE^e	Adiabatic ^f
HMIN1	−17.02	−16.26	−16.14	−15.97	0.89	−15.08
HTS1	−16.57	−15.78	−15.74	−15.62	0.62	−15.00
HTS2	−15.45	−15.04	−14.98	−14.82	0.59	−14.23
FSMIN	−1.81	−3.25	−2.87	−2.73	0.47	−2.27
HBTS	1.54	0.80	1.06 ^g	1.14 ^g	0.26 ^g	1.40 ^g
PreMIN	−16.35	−15.73	−15.72	−15.57	0.79	−14.78
WaldenTS	−14.39	−13.03	−13.33	−13.24	0.62	−12.62
FSTS1	18.84	19.20	19.19	19.40	0.48	19.88
FSTS2	18.12	17.44	17.80	18.07	0.85	18.93
DITS	9.64	9.13	9.61	9.82	−0.02	9.81
PostHMIN	−68.49	−65.91	−65.58	−65.61	3.26	−62.34
WaldenPostHMIN	−57.10	−53.75 ^h	−53.44 ^h	−53.55 ^h	2.48 ^h	−51.07 ^h
ABSTS	−14.49	−13.79	−13.59	−13.43	0.45	−12.98
ABSMIN2	3.08	2.71	3.03	3.23	0.52	3.75
PostTS	−38.33	−27.93	−27.17	−27.01	−3.75	−30.76
PostDHMIN	−141.29	−136.29	−135.89	−136.00	5.14	−130.86
HOO [−] + CH ₃ Br	MP2 ^a	DZ ^b	TZ ^c	QZ ^d	ΔZPE^e	Adiabatic ^f
HMIN1	−17.61	−17.21	−16.92	−16.74	0.74	−15.99
HMIN2	−17.22	−16.57 ^h	−16.18 ^h	−15.97 ^h	0.82 ^h	−15.15 ^h
HTS1	−17.13	−16.72	−16.49	−16.35	0.54	−15.81
HTS2	−15.90	−15.92	−15.71	−15.53	0.42	−15.11
FSMIN	−10.48	−11.07	−10.89	−10.76	0.37	−10.39
HBTS	−0.36	−0.67	−0.70 ^g	−0.62 ^g	0.39 ^g	−0.23 ^g
PreMIN	−16.87	−16.88	−16.73	−16.57	0.79	−15.77
WaldenTS	−16.35	−16.41	−16.45	−16.32	0.62	−15.70
FSTS1	14.09	12.96	12.98	13.17	0.78	13.95
FSTS2	14.10	13.18 ^h	13.29 ^h	13.55 ^h	0.95 ^h	14.50 ^h
DITS	7.23	6.88	7.42	7.69	0.05	7.73
PostHMIN	−72.09	−71.45	−70.85	−70.93	3.71	−67.22
ABSTS	−15.27	−14.80	−14.48	−14.30	0.41	−13.89
ABSMIN1	−11.03	−11.55	−11.18	−10.89	0.00	−10.90
ABSMIN2	0.38	−0.79	−0.37	−0.12	0.57	0.45
PostTS	−40.96	−28.82	−27.82	−27.63	−4.16	−31.80
PostDHMIN	−144.57	−141.54	−140.79	−140.94	5.48	−135.46
HOO [−] + CH ₃ I	MP2 ^a	DZ ^b	TZ ^c	QZ ^d	ΔZPE^e	Adiabatic ^f
HMIN1	−18.52	−18.05	−17.75	−17.57	0.72	−16.84
HMIN2	−18.45	−17.96	−17.60	−17.40	0.79	−16.61
HTS1	−18.02	−17.56	−17.31	−17.17	0.53	−16.64
HTS2	−16.44	−16.51	−16.27	−16.10	0.54	−15.56
FSMIN	−22.36	−22.28	−22.11	−22.03	0.44	−21.59
HBTS	−2.65	−3.19	−3.37	−3.30	0.40	−2.90
FSTS1	9.16	7.85	7.91	8.04	0.87	8.91
FSTS2	10.01	8.46 ^h	8.67 ^h	8.93 ^h	1.08 ^h	10.01 ^h
DITS	3.40	2.68	3.11	3.36	0.19	3.55



Table 1 (continued)

HOO [−] + CH ₃ I	MP2 ^a	DZ ^b	TZ ^c	QZ ^d	ΔZPE ^e	Adiabatic ^f
PostHMIN	−75.63	−75.15	−74.52	−74.74	3.94	−70.80
ABSTS	−16.32	−15.83	−15.48	−15.30	0.28	−15.02
ABSMIN1	−14.52	−14.76	−14.42	−14.15	0.28	−13.88
ABSMIN2	−2.98	−4.37	−3.97	−3.75	0.66	−3.09
PostTS	−36.02	−27.58	−26.36	−26.15	−4.08	−30.23
PostDHMIN	−147.56	−144.70	−143.92	−144.19	5.79	−138.40

^a MP2/aug-cc-pVDZ. ^b CCSD(T)-F12b/aug-cc-pVDZ. ^c CCSD(T)-F12b/aug-cc-pVTZ. ^d CCSD(T)-F12b/aug-cc-pVQZ at CCSD(T)-F12b/aug-cc-pVTZ geometry. ^e ΔZPE[CCSD(T)-F12b/aug-cc-pVTZ]. ^f QZ + ΔZPE. ^g CCSD(T)-F12b/aug-cc-pVDZ geometry and frequencies. ^h MP2/aug-cc-pVDZ geometry and frequencies.

III. Results and discussion

The complex PESs of the HOO[−] + CH₃Y [Y = F, Cl, Br and I] reactions showing the benchmark classical (adiabatic) relative energies of the stationary points along the considered pathways are presented in Fig. 1. The *ab initio* energies determined at the MP2/aug-cc-pVDZ and CCSD(T)-F12b/aug-cc-pVnZ [*n* = 2, 3 and 4] levels of theory are summarized in Tables 1 and 2. Taking a cue from previous studies on the HOO[−]/ClO[−] + CH₃Cl and HO[−] + CH₃F reactions,^{40,65,69,95} in addition to the typical S_N2 (CH₃OOH + Y[−]) and proton-abstraction (CH₂Y[−] + H₂O₂) routes, alternative channels of peroxide ion substitution (CH₃OO[−] + HY), S_N2-induced elimination (CH₂O + HY + HO[−]) and S_N2-induced rearrangement (CH₂(OH)O[−] + HY) are also analyzed. It should be noted that in the case of the HOO[−] + CH₃Cl reaction, the dynamical characterization reported by Xie and co-workers did not reveal the existence of the corresponding peroxide ion substitution, S_N2-induced rearrangement and proton abstraction, presumably, due to the fact that overall 1154 trajectories were run at one sole collision energy of 0.9 kcal mol^{−1}.⁹⁵ However, the pathways of peroxide ion substitution and S_N2-induced rearrangement were also considered in the course of their stationary-point survey.

As seen in Fig. 1, in the entrance channel of the back-side attack Walden inversion, several H-bonded stationary points can be found for HOO[−] + CH₃Y: HMIN1 [Y = F, Cl, Br and I], HTS1 [Y = F, Cl, Br and I], HMIN2 [Y = Br and I] and HTS2 [Y = Cl, Br and I]. The energetics of these minima and transition states are similar, and the differences in the relative energies are within ~1.5 kcal mol^{−1}. Moreover, the typical PreMIN ion-dipole complex does not demonstrate notable distinctions, as well. On the other hand, for the alternative pre-reaction halogen-bonded complex pathway, a different situation can be found. In line with HO[−] + CH₃Y,^{24,38} FSMIN is situated above HMIN1 by 13.2 (12.8) and 6.0 (5.6) kcal mol^{−1} for Y = Cl and Br, in order; while for Y = I, FSMIN is below HMIN1 by 4.5 (4.7) kcal mol^{−1}. Note that the back-side attack Walden-inversion mechanism is submerged except for Y = F, where HBTS is positioned above the reactant asymptote by 1.1 (1.4) kcal mol^{−1}. With the atomic number of Y, the barrier height of HBTS is increasing: 3.9 (3.7), 10.1 (10.2) and 18.7 (18.7) kcal mol^{−1} relative to the corresponding FSMIN, for Y = F, Cl, Br and I, respectively. The deep well of the FSMIN complex at Y = I points out the common occurrence of the front-side complex formation mechanism in

S_N2 reactions involving CH₃I.^{48,60,109} The energy profile of the conventional stationary points of the Walden-inversion pathway (PreMIN → WaldenTS → WaldenPostMIN/PostHMIN) is also profoundly comparable with that of the HO[−] case.^{24,38} For instance, the classical (adiabatic) barrier heights of WaldenTS are 10.3 (10.1), 2.3 (2.2) and 0.2 (0.1) kcal mol^{−1} for Y = F, Cl and Br, respectively, while in the case of HO[−] at the same level of theory, these values are 11.2 (11.4), 2.4 (2.4) and 0.2 (0.1) kcal mol^{−1}, in the same order. The global minimum of S_N2 is also located at PostHMIN, although, compared to HO[−] + CH₃Y, higher classical energies of −49.7, −65.6, −70.9 and −74.7 kcal mol^{−1} can be determined for HOO[−] in the case of Y = F, Cl, Br and I, respectively. In tandem with this, a notable disparity emerges in the reaction enthalpies of the S_N2 channels: HOO[−] + CH₃Y happens to be more endothermic by exactly 6.1 kcal mol^{−1} in all cases. As a result, in the case of the S_N2 reactions of HOO[−], larger dissociation energies can be observed for the leaving Y[−] at PostHMIN, indicating a more significant post-reaction hydrogen-bonded complex formation. Here, one may highlight the relevance of peroxide ion substitution, as well, because the formation of the CH₃OO[−] + HY products is also more exothermic than that of the HO[−] cases, predicting a substantially increased probability for peroxide ion substitution, especially for HOO[−] + CH₃F.⁴⁰ WaldenPostHMIN also plays a significant role, as Zhao *et al.*⁹⁵ uncovered, and the reaction can proceed through this minimum towards PostTS, leading to the unusual CH₂O + HY + HO[−] products. In the case of Y = Cl, WaldenPostHMIN could not be identified at the CCSD(T)-F12b/aug-cc-pVnZ [*n* = 2, 3] levels of theory. It is noteworthy that for Y = F, the novel mechanism of S_N2-induced elimination is exceedingly more exothermic than S_N2, submerged by 29.9 (36.3) kcal mol^{−1}. The global minimum of the PES is situated at the double H-bonded PostDHMIN complex, and the most exothermic process corresponds to the S_N2-induced rearrangement channel, but it is supposedly an improbable reaction route considering the multiple bond-breaking and -forming processes involved. Concerning the S_N2 pathways that result in the retention of the initial CH₃Y configuration, two different transition states (FSTS1 and FSTS2) can be identified for front-side attacks. According to the study of Ma *et al.*,¹¹⁰ double inversion may not be an IRC path through a DITS-like transition state; despite that, theoretical investigations underscored its crucial character in the mechanism.^{111,112} Similarly to the HO[−] case, the transition state of double inversion has lower energy than that of front-side attack; however, no submerged DITS can be obtained.^{24,38} The most endothermic channel is proton abstraction with reaction enthalpies



Table 2 The best available experimental and our benchmark *ab initio* 0 K reaction enthalpies (kcal mol^{−1}) of several product channels for the HOO[−] + CH₃Y [Y = F, Cl, Br, I] reactions

	MP2	CCSD(T)-F12b						
HOO [−] + CH ₃ F	DZ ^a	DZ ^b	TZ ^c	QZ ^d	ΔZPE ^e	Adiabatic ^f	Experiment ^g	
CH ₃ OOH + F [−]	−18.24	−13.38	−13.06	−13.13	1.46	−11.67	−11.82 ± 0.14	
CH ₂ F [−] + H ₂ O ₂	34.54	34.87	35.22	35.32	−1.84	33.48	—	
CH ₃ OO [−] + HF	−11.24	−10.28	−10.08	−10.02	−1.11	−11.12	−11.00 ± 0.15	
CH ₂ O + HF + HO [−]	−51.98	−43.50	−42.94	−43.06	−4.92	−47.98	−47.99 ± 0.10	
CH ₂ (OH)O [−] + HF	−85.40	−79.85	−79.22	−79.15	−0.70	−79.85	—	
HOO [−] + CH ₃ Cl	MP2 ^a	DZ ^b	TZ ^c	QZ ^d	ΔZPE ^e	Adiabatic ^f	Experiment ^g	
CH ₃ OOH + Cl [−]	−48.79	−45.72	−45.61	−45.83	2.44	−43.39	−43.07 ± 0.14	
CH ₂ Cl [−] + H ₂ O ₂	22.01	21.82	21.80	21.81	−1.33	20.48	21.64 ± 0.49	
CH ₃ OO [−] + HCl	−3.64	−3.44	−3.10	−2.89	−1.77	−4.66	−4.31 ± 0.14	
CH ₂ O + HCl + HO [−]	−44.38	−36.66	−35.97	−35.93	−5.58	−41.51	−41.30 ± 0.09	
CH ₂ (OH)O [−] + HCl	−77.81	−73.01	−72.24	−72.02	−1.36	−73.39	—	
HOO [−] + CH ₃ Br	MP2 ^a	DZ ^b	TZ ^c	QZ ^d	ΔZPE ^e	Adiabatic ^f	Experiment ^g	
CH ₃ OOH + Br [−]	−54.91	−54.21	−53.65	−53.98	2.85	−51.14	−50.60 ± 0.14	
CH ₂ Br [−] + H ₂ O ₂	18.32	16.94	17.14	17.15	−1.17	15.98	—	
CH ₃ OO [−] + HBr	−0.72	−1.04	−0.51	−0.37	−1.86	−2.23	−1.85 ± 0.14	
CH ₂ O + HBr + HO [−]	−41.46	−34.26	−33.37	−33.41	−5.68	−39.08	−38.84 ± 0.10	
CH ₂ (OH)O [−] + HBr	−74.89	−70.61	−69.65	−69.50	−1.46	−70.96	—	
HOO [−] + CH ₃ I	MP2 ^a	DZ ^b	TZ ^c	QZ ^d	ΔZPE ^e	Adiabatic ^f	Experiment ^g	
CH ₃ OOH + I [−]	−61.29	−60.78	−60.32	−60.89	3.25	−57.64	−56.97 ± 0.14	
CH ₂ I [−] + H ₂ O ₂	13.49	11.84	11.92	11.84	−0.95	10.89	—	
CH ₃ OO [−] + HI	2.44	1.68	2.14	2.24	−1.93	0.32	0.83 ± 0.14	
CH ₂ O + HI + HO [−]	−38.30	−31.54	−30.72	−30.80	−5.74	−36.54	−36.16 ± 0.10	
CH ₂ (OH)O [−] + HI	−71.72	−67.89	−67.00	−66.89	−1.52	−68.41	—	

^a MP2/aug-cc-pVDZ. ^b CCSD(T)-F12b/aug-cc-pVDZ. ^c CCSD(T)-F12b/aug-cc-pVTZ. ^d CCSD(T)-F12b/aug-cc-pVQZ at CCSD(T)-F12b/aug-cc-pVTZ geometry. ^e ΔZPE(CCSD(T)-F12b/aug-cc-pVTZ). ^f QZ + ΔZPE. ^g Data obtained from the latest version (1.130) of the Active Thermochemical Tables (ATcT).^{113,114} The uncertainties are derived using the Gaussian error-propagation law on the uncertainties of each 0 K enthalpy of formation provided in ATcT.

of 33.5 (F), 20.5 (Cl), 16.0 (Br) and 10.9 (I) kcal mol^{−1}. The entrance channel of proton abstraction is found to be the same as that for S_N2 and is supported by IRC calculations, in which three stationary points (two minima and one transition state) are explored along the pathway: ABSTS [Y = F, Cl, Br and I], ABSMIN1 [Y = Br and I], and ABSMIN2 [Y = F, Cl, Br and I].

The structures of the stationary points featuring the selected bond lengths and angles are shown in Fig. 2. The associated stationary points in the reactant channels (HMIN1/HTS1 and HMIN2/HTS2) demonstrate slight differences in their geometries, and the most pronounced disparity is discerned in the orientation of the corresponding HOO[−] group. Regarding WaldenTS, two distinct structures are characterized depending on Y: the dihedral angle of O–O···C–H is ~180° (*trans* arrangement) at Y = F, whereas a value of ~0° (*cis* arrangement) is obtained at Y = Cl and Br, as seen in Fig. 2. According to earlier investigations on S_N2 reactions, similar discrepancies observed at CH₃F are not uncommon;²⁴ for instance, in the case of HO[−] + CH₃Y,³⁸ for Y = Cl, Br and I FSTS has C_s symmetry, while for Y = F, the symmetry is broken. It should be noted that previous studies on the HOO[−] + CH₃Cl S_N2 reaction reported a *trans* alignment for the O–O···C–H torsion angle of WaldenTS computed at the MP2/6-311++G(d,p) level of theory.^{96,97} The geometries of PreMIN and WaldenTS defined in the early work of

Evanseck *et al.* are discrepant from our benchmark results due to their implemented symmetry-constrained geometry optimizations.⁷⁴ Moreover, Ren *et al.* revealed two different transition states for Walden inversion with a *trans* alignment of the corresponding O–O···C–H torsion angle for both cases.⁷⁸ Nevertheless, in other investigations, the geometry of the uncovered WaldenTS of HOO[−] + CH₃Cl is in accordance with that presented in this benchmark work.^{79,88,95} It should also be highlighted that Wu *et al.* identified PreMIN and WaldenTS for Y = I at the MP2/6-311++G(d,p) level of theory,⁹⁶ although, in the course of the present study, WaldenTS cannot be found for Y = I at the MP2/aug-cc-pVDZ and CCSD(T)-F12b/aug-cc-pVnZ [*n* = 2, 3] levels of theory. Hence, the issues regarding these stationary points underline the relevance of employing higher-level *ab initio* methods for theoretical investigations. Concerning PostHMIN, alternative conformational isomers cannot be determined in contrast to the HO[−] + CH₃F reaction.⁴⁰ As shown in Fig. 2, the transition states of the front-side attack mechanism differ from each other in the orientation of the HOO[−] group, and owing to the additional Y···HO bond, FSTS2 is below FSTS1 in the case of Y = F and Cl. It is noteworthy that all the stationary-point characterizations can be performed without imposing symmetry restrictions, except for ABSMIN1, which has C_s symmetry. There are cases, where a C_s symmetry



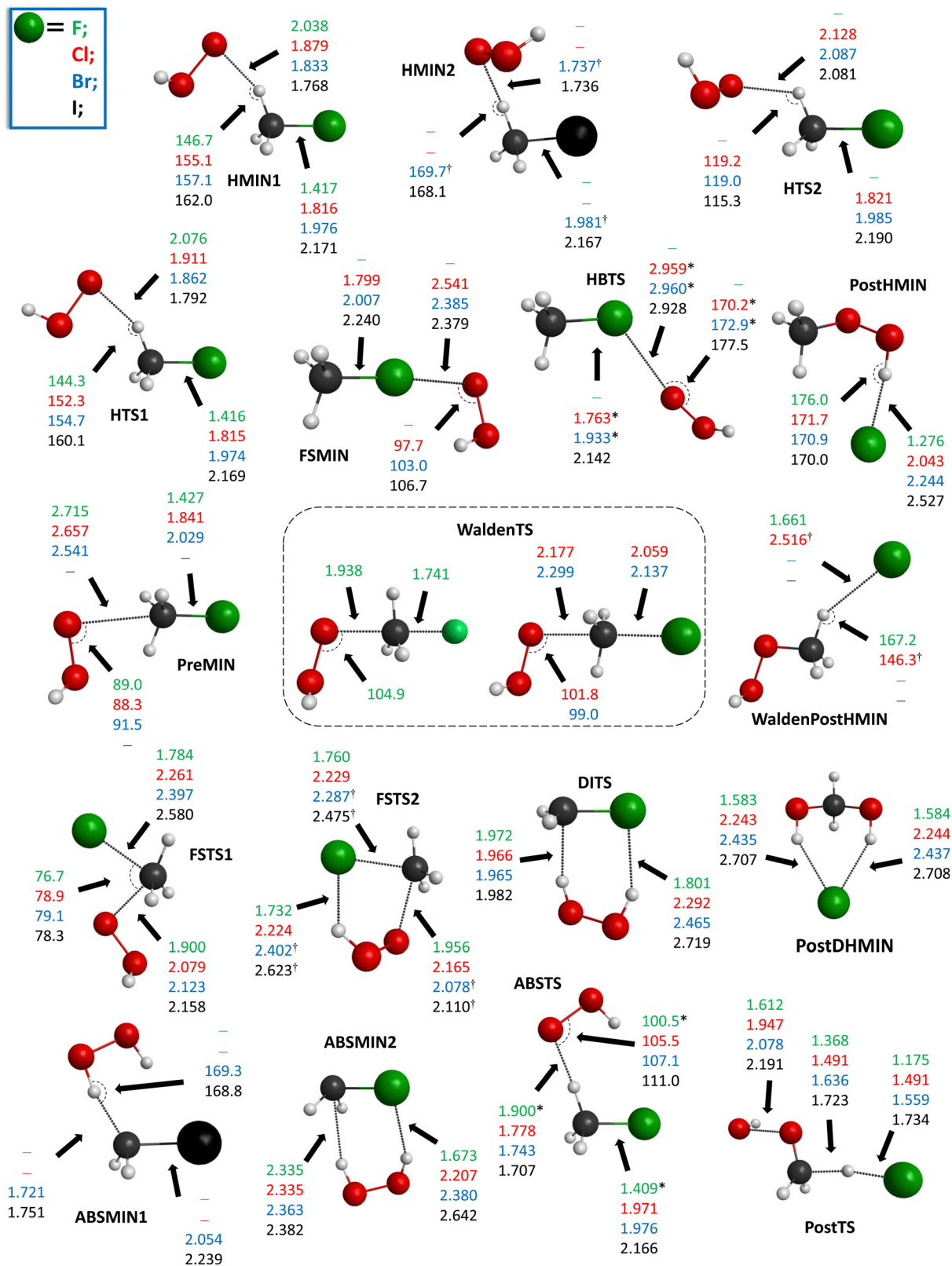


Fig. 2 Structures of the stationary points of the $\text{HOO}^- + \text{CH}_3\text{Y}$ [$\text{Y} = \text{F}, \text{Cl}, \text{Br}, \text{I}$] reactions showing the most important bond lengths (Å) and angles (°) obtained at the CCSD(T)-F12b/aug-cc-pVTZ level of theory. † MP2/aug-cc-pVDZ structure; *CCSD(T)-F12b/aug-cc-pVDZ structure. Note that for $\text{Y} = \text{F}$ at WaldenTS, a distinct structure can be identified compared to the case of $\text{Y} = \text{Cl}$ and Br .

would also be expected (e.g., HTS1, ABST5); however, the corresponding geometry optimizations do not converge. The most accurate, CCSD(T)-F12b/aug-cc-pVTZ Cartesian coordinates of the stationary points, as well as of reactants and products, are provided in the ESI.†

The calculated classical and adiabatic *ab initio* relative energies of the products and the available “experimental” reaction enthalpies obtained from the active thermochemical tables (ATcT)^{113,114} are given in Table 2. The benchmark structures of the reactants and products are shown in Fig. 3. The reaction enthalpies of S_N2 and proton abstraction decrease with increasing atomic weight of Y, whereas for the other pathways, a reverse tendency is revealed. Alongside the proton-abstraction channels for Y = F, Cl, Br and I, peroxide ion substitution is also an endothermic pathway in the case of Y = I. It is notable that for Y = F, the difference between the reaction enthalpies of S_N2 and peroxide ion substitution is only 0.5 kcal mol^{−1}. In most instances, our benchmark results are in satisfactory agreement with the experimental data, except for the $\text{CH}_2\text{Cl}^- + \text{H}_2\text{O}_2$ products, where a difference of 1.2 kcal mol^{−1} emerges. However, it should be noted that the derived uncertainty of the experimental reaction enthalpy is remarkably substantial (± 0.5 kcal mol^{−1}). Similarly, for the $\text{F}^- + \text{CH}_3\text{Cl} \rightarrow \text{CH}_2\text{Cl}^- + \text{HF}$ proton-abstraction channel, a large deviation (0.9 kcal mol^{−1}) can also be observed between the experimental and our calculated benchmark reaction enthalpy with a significant uncertainty (0.5 kcal mol^{−1}) of the experimental value.¹¹² Thus, these cases may highlight the inaccuracy of the available 0 K enthalpy of formation for CH_2Cl^- in the ATcT. In the case of the $\text{HOO}^- + \text{CH}_3\text{Y}$ [Y = F and Cl] S_N2 reactions, the reaction energies of −13.0 (F) and −45.3 (Cl) kcal mol^{−1}, obtained by Wu *et al.* utilizing CCSD(T)/aug-cc-pVTZ(-PP) energy calculations at the MP2/6-311++G(d,p) geometries,⁹⁶ in kcal mol^{−1} are in conformity with our benchmark values of −13.0 (F) and −45.8 (Cl) kcal mol^{−1}. Although, for Y = Br and I, their S_N2 reaction energies of −50.9 and −56.4 kcal mol^{−1} are higher than our results by 3.1 and 4.5 kcal mol^{−1}, respectively. The classical

energies of the stationary points of the present work can also be compared with the results of Wu *et al.*⁹⁶ They characterized five stationary points (HMIN1, HTS2, PreMIN, WaldenTS and PostHMIN) along the back-side attack Walden inversion, mainly, their computed CCSD(T)/aug-cc-pVTZ(-PP) energies are in good agreement with our benchmark data. In an earlier study on $\text{HOO}^- + \text{CH}_3\text{Cl}$ by Zhao *et al.*,⁹⁵ the reported energies of PreMIN and PostHMIN at the MP2/6-31+G(d,p) level of theory are in good agreement with the present benchmark values. For WaldenTS, a difference of more than 2 kcal mol^{−1} occurs; moreover, an enormous deviation of 13.2 kcal mol^{−1} is obtained at Walden-PostHMIN, remarkably. Motivated by this discrepancy, we characterized the corresponding stationary points of $\text{HOO}^- + \text{CH}_3\text{Cl}$ at the MP2/6-31+G(d,p) level of theory using the Molpro program package.¹⁰⁸ In the course of computations, spherical harmonic basis functions are used; however, it is noteworthy that by employing Cartesian functions, comparable relative energies can be obtained within ± 0.3 kcal mol^{−1}. Our obtained MP2/6-31+G(d,p) classical energies of −14.9 (PreMIN), −10.5 (WaldenTS), −64.6 (PostHMIN), −53.2 (WaldenPostHMIN), −31.5 (PostTS), and −136.5 (PostDHMIN), in kcal mol^{−1}, are in conformity with the benchmark data. While our optimized structures of the stationary points show satisfactory alignment with those determined by Zhao *et al.*,⁹⁵ significant inexplicable disparities are unveiled for the classical energies in a few cases. We also determined the classical (adiabatic) energies of the products at the MP2/6-31+G(d,p) level; $\text{CH}_2\text{Cl}^- + \text{H}_2\text{O}_2$: 29.4 (27.7), $\text{CH}_3\text{OOH} + \text{Cl}^-$ −45.7 (−43.5), $\text{CH}_3\text{OO}^- + \text{HCl}$ −2.1 (−3.7), $\text{CH}_2\text{O} + \text{HCl} + \text{HO}^-$ −40.0 (−45.8) and $\text{CH}_2(\text{OH})\text{O}^- + \text{HCl}$ −75.2 (−76.8), in kcal mol^{−1}. It can be seen that for certain cases, the provided energies differ from the experiment by more than 4 kcal mol^{−1}; especially for proton abstraction, an enormous difference of 6.1 kcal mol^{−1} occurs, which casts doubt on the reliability of MP2/6-31+G(d,p). The G2+ adiabatic energies of WaldenTS (−13.5 kcal mol^{−1}) and the S_N2 products (−43.2 kcal mol^{−1}), computed by Ren *et al.* for $\text{HOO}^- + \text{CH}_3\text{Cl}$, are also in consonance with the present study.⁷⁹

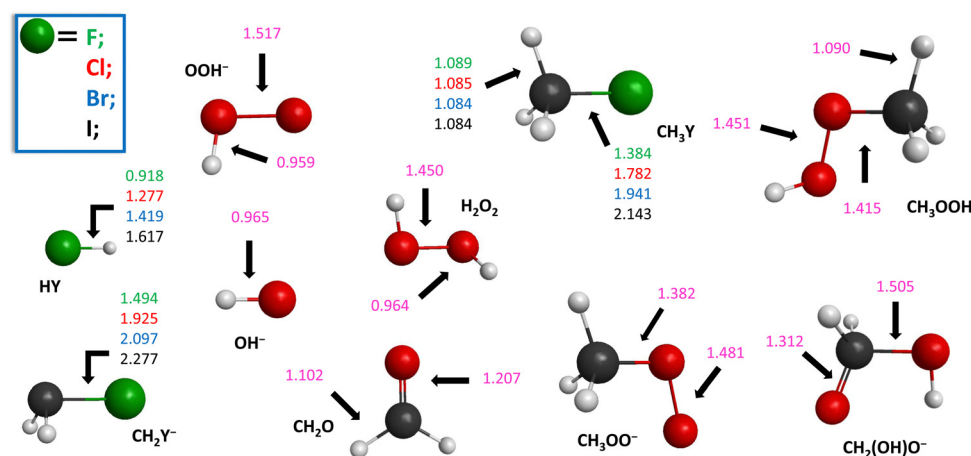


Fig. 3 Structures of the reactants and products of the $\text{HOO}^- + \text{CH}_3\text{Y}$ [Y = F, Cl, Br, I] reactions showing the most important bond lengths (Å) obtained at the CCSD(T)-F12b/aug-cc-pVTZ level of theory.



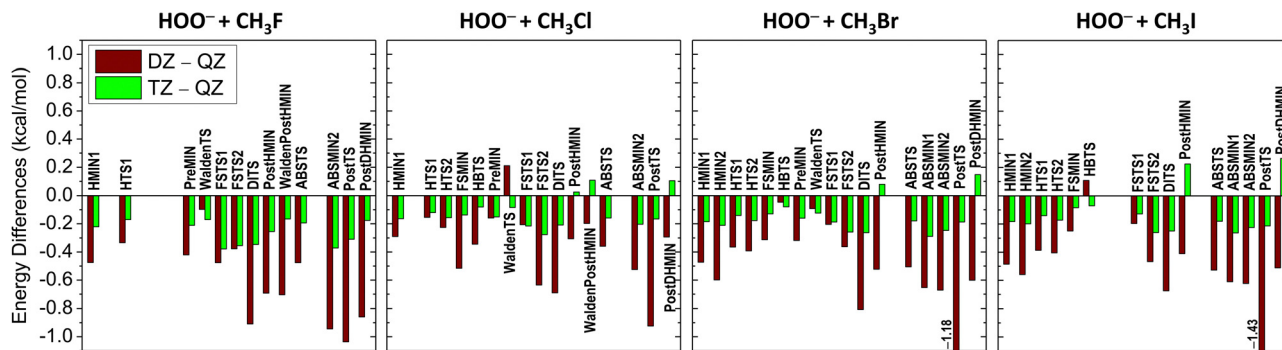


Fig. 4 Convergence of the CCSD(T)-F12b relative energies for the stationary points of the $\text{HOO}^- + \text{CH}_3\text{Y}$ [$\text{Y} = \text{F}, \text{Cl}, \text{Br}, \text{I}$] reactions utilizing the aug-cc-pVDZ (DZ), aug-cc-pVTZ (TZ) and aug-cc-pVQZ (QZ) basis sets.

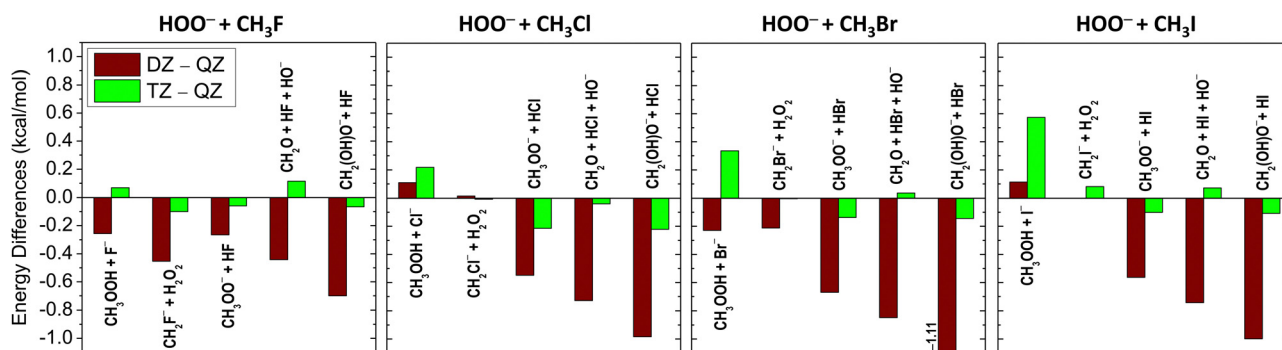


Fig. 5 Convergence of the CCSD(T)-F12b relative energies for the product channels of the $\text{HOO}^- + \text{CH}_3\text{Y}$ [$\text{Y} = \text{F}, \text{Cl}, \text{Br}, \text{I}$] reactions utilizing the aug-cc-pVDZ (DZ), aug-cc-pVTZ (TZ) and aug-cc-pVQZ (QZ) basis sets.

As shown in Fig. 4 and 5, the basis-set convergence of the CCSD(T)-F12b relative energies is also investigated for the title reactions. In most cases, a fast and smooth basis-set convergence can be recognized, except for WaldenTS [$\text{Y} = \text{F}$ and Br], HBTS [$\text{Y} = \text{Br}$], FST1 [$\text{Y} = \text{Cl}$] and $\text{CH}_3\text{OOH} + \text{Y}^-$ [$\text{Y} = \text{Cl}, \text{Br}$ and I], as in these instances the relative energy differences between aug-cc-pVDZ (DZ) and aug-cc-pVQZ (QZ) are smaller than the corresponding values of aug-cc-pVTZ (TZ) and QZ. The largest differences emerge at PostTS [$\text{Y} = \text{Br}$ and I] and $\text{CH}_2(\text{OH})\text{O}^- + \text{HBr}$, where the deviations between the DZ and QZ relative energies are found to be in the range of 1.1–1.4 kcal mol^{-1} . In contrast, the energy differences between TZ and QZ are within $\pm 0.4 \text{ kcal mol}^{-1}$, except at $\text{CH}_3\text{OOH} + \text{I}^-$ ($0.57 \text{ kcal mol}^{-1}$). Regarding the ZPE effects, the most significant contributions appear at the post-reaction stationary points (PostHMIN, WaldenPostHMIN, PostTS and PostDHMIN) and for the products of $\text{CH}_3\text{OOH} + \text{Y}^-$ and $\text{CH}_2\text{O} + \text{HY} + \text{HO}^-$. The vast majority of the stationary points have positive ZPE corrections, whereas, in the case of the reaction channels, positive ZPE effects occur only for the $\text{CH}_3\text{OOH} + \text{Y}^-$ products.

IV. Summary and conclusions

In this study, we have characterized the complex potential energy surfaces of the $\text{HOO}^- + \text{CH}_3\text{Y}$ [$\text{Y} = \text{F}, \text{Cl}, \text{Br}$ and I] reactions using the modern explicitly-correlated CCSD(T)-F12b

method with the aug-cc-pVnZ [$n = 2-4$] basis sets. For $\text{S}_{\text{N}}2$, we have considered the pathways of back-side attack Walden inversion, front-side attack, double inversion¹⁹ and halogen-bonded complex formation.⁴⁸ In most cases, the entrance channel of $\text{HOO}^- + \text{CH}_3\text{Y}$ comprises seven stationary points: two H-bonded, a front-side halogen-bonded and a traditional ion-dipole minima, as well as two H-bonded and front-side halogen-bonded transition states. Similar to the $\text{HO}^- + \text{CH}_3\text{Y}$ $\text{S}_{\text{N}}2$ reactions,^{24,38} no typical transition state has been identified for the Walden inversion in the case of $\text{Y} = \text{I}$, and in light of the discrepancy of the earlier findings, we have clarified the accurate structure of the Walden-inversion transition state for $\text{Y} = \text{Cl}$. In the exit channel of $\text{S}_{\text{N}}2$, two H-bonded minima are situated: $\text{Y}^- \cdots \text{HOOCH}_3$ and $\text{Y}^- \cdots \text{HCH}_2\text{OOH}$. Based on the findings of Xie and co-workers,⁹⁵ the $\text{HOO}^- + \text{CH}_3\text{Cl}$ reaction can proceed through $\text{Cl}^- \cdots \text{HCH}_2\text{OOH}$ towards the $[\text{Cl} \cdots \text{H} \cdots \text{CH}_2\text{O} \cdots \text{OH}]^-$ transition state generating the unusual products of $\text{CH}_2\text{O} + \text{HCl} + \text{HO}^-$. It should be highlighted that for $\text{HOO}^- + \text{CH}_3\text{F}$, the reaction enthalpy of this novel $\text{S}_{\text{N}}2$ -induced elimination is more negative by $36.3 \text{ kcal mol}^{-1}$ than the corresponding $\text{S}_{\text{N}}2$ process. Concerning the retention paths of $\text{S}_{\text{N}}2$, two distinct transition states have been recognized for front-side attacks, and as observed for $\text{HO}^- + \text{CH}_3\text{Y}$, double inversion is a lower-energy process than front-side attack.^{24,38} Building upon the earlier work of Xie and co-workers,⁹⁵ besides $\text{S}_{\text{N}}2$ -induced elimination, we have also investigated other channels such as proton abstraction ($\text{CH}_2\text{Y}^- + \text{H}_2\text{O}_2$), peroxide ion substitution ($\text{CH}_3\text{OO}^- + \text{HY}$) and



S_N2 -induced rearrangement ($\text{CH}_2(\text{OH})\text{O}^- + \text{HY}$). In the case of $\text{Y} = \text{F}, \text{Cl}$ and Br , the peroxide ion substitution has been found to be exothermic with reaction enthalpies of -11.1 (F), -4.7 (Cl) and -2.2 (Br) kcal mol^{-1} . The most exothermic path is S_N2 -induced rearrangement; however, it is presumed to be an improbable reaction channel due to the complex bond-breaking and -forming processes involved. The benchmark reaction enthalpies presented in this work are usually in excellent agreement with those obtained from ATcT.^{113,114} We have also assessed the basis-set convergence of the CCSD(T)-F12b method and the ZPE contributions of the stationary points.

We are confident that the present benchmark characterization of $\text{HOO}^- + \text{CH}_3\text{Y}$ supports further theoretical and experimental investigations regarding reaction dynamics as well as the influence of the α -effect related to HOO^- .

Conflicts of interest

There are no conflicts of interest to declare.

Acknowledgements

We acknowledge the financial support of the National Research, Development and Innovation Office-NKFIH, K-125317 and K-146759; project no. TKP2021-NVA-19 provided by the Ministry of Innovation and Technology of Hungary from the National Research, Development and Innovation Fund, financed under the TKP2021-NVA funding scheme; the National Young Talent Scholarship (Grant no. NTP-NFTÖ-22-B-0050 for D. A. T.); and the Momentum (Lendület) Program of the Hungarian Academy of Sciences.

References

- 1 A. Dedieu and A. Veillard, *J. Am. Chem. Soc.*, 1972, **94**, 6730.
- 2 W. N. Olmstead and J. I. Brauman, *J. Am. Chem. Soc.*, 1977, **99**, 4219.
- 3 A. Merkel, R. Zahradník and Z. Havlas, *J. Am. Chem. Soc.*, 1988, **110**, 8355.
- 4 S. S. Shaik, H. B. Schlegel and S. Wolfe, *Theoretical Aspects of Physical Organic Chemistry: The S_N2 Mechanism*, Wiley, New York, 1992.
- 5 W. L. Hase, *Science*, 1994, **266**, 998.
- 6 M. L. Chabinye, S. L. Craig, C. K. Regan and J. I. Brauman, *Science*, 1998, **279**, 1882.
- 7 J. K. Laerdahl and E. Uggerud, *Int. J. Mass Spectrom.*, 2002, **214**, 277.
- 8 E. Uggerud, *Adv. Phys. Org. Chem.*, 2017, **51**, 1.
- 9 T. A. Hamlin, M. Swart and F. M. Bickelhaupt, *ChemPhysChem*, 2018, **19**, 1315.
- 10 R. Wester, *Mass Spectrom. Rev.*, 2022, **41**, 627.
- 11 A. J. R. Heck and D. W. Chandler, *Annu. Rev. Phys. Chem.*, 1995, **46**, 335.
- 12 M. N. R. Ashfold, N. H. Nahler, A. J. Orr-Ewing, O. P. J. Vieuxmaire, R. L. Toomes, T. N. Kitsopoulos, I. A. Garcia, D. A. Chestakov, S. M. Wu and D. H. Parker, *Phys. Chem. Chem. Phys.*, 2006, **8**, 26.
- 13 D. C. Clary, *Proc. Natl. Acad. Sci. U. S. A.*, 2008, **105**, 12649.
- 14 J. Mikosch, S. Trippel, C. Eichhorn, R. Otto, U. Lourderaj, J. X. Zhang, W. L. Hase, M. Weidemüller and R. Wester, *Science*, 2008, **319**, 183.
- 15 J. Meyer and R. Wester, *Annu. Rev. Phys. Chem.*, 2017, **68**, 333.
- 16 J. Li, B. Zhao, D. Xie and H. Guo, *J. Phys. Chem. Lett.*, 2020, **11**, 8844.
- 17 J. I. Brauman, *Science*, 2008, **319**, 168.
- 18 P. Manikandan, J. Zhang and W. L. Hase, *J. Phys. Chem. A*, 2012, **116**, 3061.
- 19 I. Szabó and G. Czako, *Nat. Commun.*, 2015, **6**, 5972.
- 20 M. Stei, E. Carrascosa, M. A. Kainz, A. H. Kelkar, J. Meyer, I. Szabó, G. Czako and R. Wester, *Nat. Chem.*, 2016, **8**, 151.
- 21 J. Xie and W. L. Hase, *Science*, 2016, **352**, 32.
- 22 L. Sun, K. Song and W. L. Hase, *Science*, 2002, **296**, 875.
- 23 L. Sun, K. Song, W. L. Hase, M. Sena and J. M. Riveros, *Int. J. Mass Spectrom.*, 2003, **227**, 315.
- 24 D. A. Tasi, Z. Fábíán and G. Czako, *Phys. Chem. Chem. Phys.*, 2019, **21**, 7924.
- 25 S. R. Hare, L. A. Bratholm, D. R. Glowacki and B. K. Carpenter, *Chem. Sci.*, 2019, **10**, 9954.
- 26 T. Tsutsumi, Y. Ono, Z. Arai and T. Taketsugu, *J. Chem. Theory Comput.*, 2020, **16**, 4029.
- 27 D. A. Tasi, C. Tokaji and G. Czako, *Phys. Chem. Chem. Phys.*, 2021, **23**, 13526.
- 28 T. Tsutsumi, Y. Ono and T. Taketsugu, *Chem. Commun.*, 2021, **57**, 11734.
- 29 T. Tsutsumi, Y. Ono and T. Taketsugu, *Top. Curr. Chem.*, 2022, **380**, 19.
- 30 S. Zhao, G. Fu, W. Zhen, L. Yang, J. Sun and J. Zhang, *Phys. Chem. Chem. Phys.*, 2022, **24**, 24146.
- 31 H. Tachikawa, M. Igarashi and T. Ishibashi, *J. Phys. Chem. A*, 2002, **106**, 10977.
- 32 H. Tachikawa and M. Igarashi, *Chem. Phys.*, 2006, **324**, 639.
- 33 H. Yin, D. Wang and M. Valiev, *J. Phys. Chem. A*, 2011, **115**, 12047.
- 34 Y. Xu, T. Wang and D. Wang, *J. Chem. Phys.*, 2012, **137**, 184501.
- 35 S. Giri, E. Echegaray, P. W. Ayers, A. S. Nuñez, F. Lund and A. Toro-Labbé, *J. Phys. Chem. A*, 2012, **116**, 10015.
- 36 J. Chen, Y. Xu and D. Wang, *J. Comput. Chem.*, 2014, **35**, 445.
- 37 T. Tsutsumi, Y. Ono, Z. Arai and T. Taketsugu, *J. Chem. Theory Comput.*, 2018, **14**, 4263.
- 38 D. A. Tasi, Z. Fábíán and G. Czako, *J. Phys. Chem. A*, 2018, **122**, 5773.
- 39 Y. G. Proenza, M. A. F. de Souza and R. L. Longo, *Chem. – Eur. J.*, 2016, **22**, 16220.
- 40 D. A. Tasi and G. Czako, *Chem. Sci.*, 2021, **12**, 14369.
- 41 J. Qin, Y. Liu and J. Li, *J. Chem. Phys.*, 2022, **157**, 124301.
- 42 R. Otto, J. Brox, S. Trippel, M. Stei, T. Best and R. Wester, *Nat. Chem.*, 2012, **4**, 534.
- 43 J. Xie, R. Otto, J. Mikosch, J. Zhang, R. Wester and W. L. Hase, *Acc. Chem. Res.*, 2014, **47**, 2960.



- 44 J. Xie, J. Zhang and W. L. Hase, *Int. J. Mass Spectrom.*, 2015, **378**, 14.
- 45 J. Xie, R. Otto, R. Wester and W. L. Hase, *J. Chem. Phys.*, 2015, **142**, 244308.
- 46 E. Carrascosa, J. Meyer and R. Wester, *Chem. Soc. Rev.*, 2017, **46**, 7498.
- 47 J. Xie, X. Ma, J. Zhang, P. M. Hierl, A. A. Viggiano and W. L. Hase, *Int. J. Mass Spectrom.*, 2017, **418**, 122.
- 48 X. Ji, C. Zhao and J. Xie, *Phys. Chem. Chem. Phys.*, 2021, **23**, 6349.
- 49 R. Otto, J. Xie, J. Brox, S. Trippel, M. Stei, T. Best, M. R. Siebert, W. L. Hase and R. Wester, *Faraday Discuss.*, 2012, **157**, 41.
- 50 J. Xie, R. Sun, M. R. Siebert, R. Otto, R. Wester and W. L. Hase, *J. Phys. Chem. A*, 2013, **117**, 7162.
- 51 J. Xie, S. C. Kohale, W. L. Hase, S. G. Ard, J. J. Melko, N. S. Shuman and A. A. Viggiano, *J. Phys. Chem. A*, 2013, **117**, 14019.
- 52 J. Xie, J. Zhang, R. Sun, R. Wester and W. L. Hase, *Int. J. Mass Spectrom.*, 2019, **438**, 115.
- 53 D. A. Tasi, T. Györi and G. Czakó, *Phys. Chem. Chem. Phys.*, 2020, **22**, 3775.
- 54 T. Györi and G. Czakó, *J. Chem. Theory Comput.*, 2020, **16**, 51.
- 55 D. A. Tasi, T. Michaelsen, R. Wester and G. Czakó, *Phys. Chem. Chem. Phys.*, 2023, **25**, 4005.
- 56 S. Rao and D. Wang, *Chin. J. Chem. Phys.*, 2023, **36**, 169.
- 57 D. A. Tasi and G. Czakó, *J. Chem. Phys.*, 2024, **160**, 044305.
- 58 E. Carrascosa, M. Bawart, M. Stei, F. Linden, F. Carelli, J. Meyer, W. D. Geppert, F. A. Gianturco and R. Wester, *J. Chem. Phys.*, 2015, **143**, 184309.
- 59 Z. Kerekes, D. A. Tasi and G. Czakó, *J. Phys. Chem. A*, 2022, **126**, 889.
- 60 D. A. Tasi and G. Czakó, *J. Chem. Phys.*, 2022, **156**, 184306.
- 61 X. Liu, S. Tian, B. Pang, H. Li and Y. Wu, *Phys. Chem. Chem. Phys.*, 2023, **25**, 14812.
- 62 X. Liu, W. Guo, H. Feng, B. Pang and Y. Wu, *J. Phys. Chem. A*, 2023, **127**, 7373.
- 63 A. Gutal and M. Paranjothy, *Phys. Chem. Chem. Phys.*, 2023, **25**, 15015.
- 64 W. P. Hu and D. G. Truhlar, *J. Am. Chem. Soc.*, 1996, **118**, 860.
- 65 S. M. Villano, N. Eyet, W. C. Lineberger and V. M. Bierbaum, *J. Am. Chem. Soc.*, 2009, **131**, 8227.
- 66 L. Junxi, W. Yanbin, Z. Qiang, L. Yu, G. Zhiyuan and W. Xiuhong, *J. Mol. Model.*, 2013, **19**, 1739.
- 67 L. Junxi, S. Qiong, L. Yu, Z. Qiang and G. Zhiyuan, *Can. J. Chem.*, 2014, **92**, 868.
- 68 L. Junxi, S. Qiong, W. Yanbin and G. Zhiyuan, *Bull. Chem. Soc. Jpn.*, 2015, **88**, 110.
- 69 F. Yu, *J. Phys. Chem. A*, 2016, **120**, 1813.
- 70 L. Yun-Yun, Q. Fang-Zhou, Z. Jun, R. Yi and L. Kai-Chung, *J. Mol. Model.*, 2017, **23**, 192.
- 71 T. Hansen, P. Vermeeren, F. M. Bickelhaupt and T. A. Hamlin, *Angew. Chem., Int. Ed.*, 2021, **60**, 20840.
- 72 S. Hoz and E. Buncel, *Isr. J. Chem.*, 1985, **26**, 313.
- 73 J. O. Edwards and R. G. Pearson, *J. Am. Chem. Soc.*, 1962, **84**, 16.
- 74 J. D. Evanseck, J. F. Blake and W. L. Jorgensen, *J. Am. Chem. Soc.*, 1987, **109**, 2349.
- 75 E. Buncel and I. H. Um, *Tetrahedron*, 2004, **60**, 7801.
- 76 C. H. DePuy, E. W. Della, J. Filley, J. J. Grabowski and V. M. Bierbaum, *J. Am. Chem. Soc.*, 1983, **105**, 2481.
- 77 E. V. Patterson and K. R. Fountain, *J. Org. Chem.*, 2006, **71**, 8121.
- 78 Y. Ren and H. Yamataka, *Org. Lett.*, 2006, **8**, 119.
- 79 Y. Ren and H. Yamataka, *Chem. – Eur. J.*, 2007, **13**, 677.
- 80 Y. Ren and H. Yamataka, *J. Org. Chem.*, 2007, **72**, 5660.
- 81 A. M. McAnoy, M. R. L. Paine and S. J. Blanksby, *Org. Biomol. Chem.*, 2008, **6**, 2316.
- 82 Y. I. Ren and H. Yamataka, *J. Comput. Chem.*, 2009, **30**, 358.
- 83 J. M. Garver, S. Gronert and V. M. Bierbaum, *J. Am. Chem. Soc.*, 2011, **133**, 13894.
- 84 J. M. Garver, Z. Yang, N. Wehres, C. M. Nichols, B. B. Worker and V. M. Bierbaum, *Int. J. Mass Spectrom.*, 2012, **330–332**, 182.
- 85 Y. Ren, X. G. Wei, S. J. Ren, K. C. Lau, N. B. Wong and W. K. Li, *J. Comput. Chem.*, 2013, **34**, 1997.
- 86 I. H. Um, L. R. Im and E. Buncel, *J. Org. Chem.*, 2010, **75**, 8571.
- 87 X. G. Wei, X. M. Sun, X. P. Wu, Y. Ren, N. B. Wong and W. K. Li, *J. Org. Chem.*, 2010, **75**, 4212.
- 88 D. L. Thomsen, J. N. Reece, C. M. Nichols, S. Hammerum and V. M. Bierbaum, *J. Am. Chem. Soc.*, 2013, **135**, 15508.
- 89 D. L. Thomsen, J. N. Reece, C. M. Nichols, S. Hammerum and V. M. Bierbaum, *J. Phys. Chem. A*, 2014, **118**, 8060.
- 90 D. L. Thomsen, C. M. Nichols, J. N. Reece, S. Hammerum and V. M. Bierbaum, *J. Am. Soc. Mass Spectrom.*, 2014, **25**, 159.
- 91 W. Y. Zhao, J. Yu, S. J. Ren, X. G. Wei, F. Z. Qiu, P. H. Li, H. Li, Y. P. Zhou, C. Z. Yin, A. P. Chen, H. Li, L. Zhang, J. Zhu, Y. Ren and K. C. Lau, *J. Comput. Chem.*, 2015, **36**, 844.
- 92 N. Singh, Y. Karpichev, R. Sharma, B. Gupta, A. K. Sahu, M. L. Satnami and K. K. Ghosh, *Org. Biomol. Chem.*, 2015, **13**, 2827.
- 93 E. Juaristi, G. Dos Passos Gomes, A. O. Terent'ev, R. Notario and I. V. Alabugin, *J. Am. Chem. Soc.*, 2017, **139**, 10799.
- 94 F. Yu, *J. Chem. Phys.*, 2018, **148**, 014302.
- 95 C. Zhao, X. Ma, X. Wu, D. L. Thomsen, V. M. Bierbaum and J. Xie, *J. Phys. Chem. Lett.*, 2021, **12**, 7134.
- 96 X. Wu, C. Zhao and J. Xie, *ChemPhysChem*, 2022, **23**, e202200285.
- 97 Y. Hu, X. Wu and J. Xie, *Phys. Chem. Chem. Phys.*, 2023, **25**, 1947.
- 98 D. J. Anick, *J. Phys. Chem. A*, 2011, **115**, 6327.
- 99 C. Möller and M. S. Plesset, *Phys. Rev.*, 1934, **46**, 618.
- 100 T. H. Dunning, *J. Chem. Phys.*, 1989, **90**, 1007.
- 101 R. Van de Vijver and J. Zádor, *Comput. Phys. Commun.*, 2020, **248**, 106947.
- 102 M. Kuwahara, Y. Harabuchi, S. Maeda, J. Fujima and K. Takahashi, *Digit. Discovery*, 2023, **2**, 1104.



- 103 E. Kraka, J. J. Antonio and M. Freindorf, *Chem. Commun.*, 2023, **59**, 7151.
- 104 K. Raghavachari, G. W. Trucks, J. A. Pople and M. Head-Gordon, *Chem. Phys. Lett.*, 1989, **157**, 479.
- 105 T. B. Adler, G. Knizia and H. J. Werner, *J. Chem. Phys.*, 2007, **127**, 221106.
- 106 G. Knizia, T. B. Adler and H. J. Werner, *J. Chem. Phys.*, 2009, **130**, 054104.
- 107 K. A. Peterson, D. Figgen, E. Goll, H. Stoll and M. Dolg, *J. Chem. Phys.*, 2003, **119**, 11113.
- 108 H.-J. Werner, P. J. Knowles, G. Knizia, F. R. Manby and M. Schütz, *et al.*, *Molpro*, version 2015.1, a package of *ab initio* programs, see <https://www.molpro.net>.
- 109 I. Szabó, B. Olsz and G. Czako, *J. Phys. Chem. Lett.*, 2017, **8**, 2917.
- 110 Y.-T. Ma, X. Ma, A. Li, H. Guo, L. Yang, J. Zhang and W. L. Hase, *Phys. Chem. Chem. Phys.*, 2017, **19**, 20127.
- 111 B. Olsz and G. Czako, *Phys. Chem. Chem. Phys.*, 2019, **21**, 1578.
- 112 G. Czako, T. Györi, B. Olsz, D. Papp, I. Szabó, V. Tajti and D. A. Tasi, *Phys. Chem. Chem. Phys.*, 2020, **22**, 4298.
- 113 B. Ruscic, R. E. Pinzon, M. L. Morton, G. Von Laszewski, S. J. Bittner, S. G. Nijsure, K. A. Amin, M. Minkoff and A. F. Wagner, *J. Phys. Chem. A*, 2004, **108**, 9979.
- 114 D. H. Ruscic and B. Bross, *Active Thermochemical Tables (ATcT) values based on ver. 1.130 of the Thermochemical Network*, 2023, available at ATcT.anl.gov.

